

Electronic Supporting Information

MOF Transmetalation beyond Cation Substitution: Defective Distortion of IRMOF-9 in the Spotlight

Stefano Canossa^{a,*},†, Luca Fornasari^{a,‡}, Nicola Demitri^b, Monica Mattarozzi^a, Duane Choquesillo-Lazarte^c, Paolo Pelagatti^a, and Alessia Bacchi^{a,*}

^a Dipartimento SCVSA, Università degli Studi di Parma, Parco Area delle scienze 11/a, 43124, Parma, Italy.

^b Elettra-Sincrotrone Trieste, S.S. 14 Km 163.5 in Area Science Park, 31149 Basovizza, Trieste, Italy.

^c Laboratorio de Estudios Cristalográficos, IACT, CSIC-UGR, Avenida de las Palmeras 4, 18100 Armilla, Granada, Spain.

† Present affiliation: Department of Chemical Engineering, Delft University of Technology, Van der Maasweg 9, 2629HZ, Delft, The Netherlands.

‡ Present affiliation: Dipartimento di Chimica “Giacomo Ciamician”, Via Selmi 2, 40126 Bologna, Italy.

* Corresponding authors

e-mail: s.canossa@tudelft.nl; alessia.bacchi@unipr.it

Contents

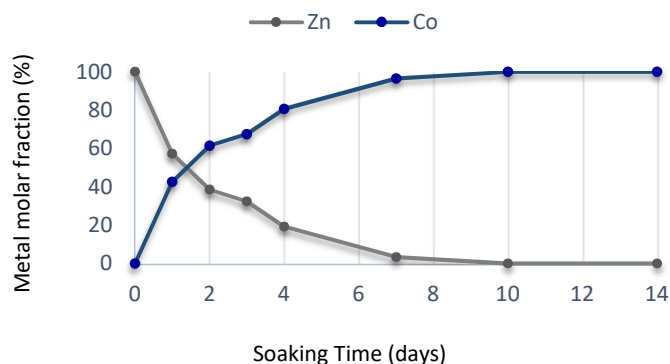
	Page
Inductively Coupled Plasma-Optical Emission Spectroscopy (ICP-OES)	
Instrumentation	2
Table S1	2
Graph S1	2
Table S2	2
Differential Scanning Calorimetry	
Instrumentation	3
Graph S2	3
Graph S3	3
Graph S4	4
Optical Microscopy	
Figure S1	4
Figure S2	4
Scanning Electron Microscopy (SEM)	
Figure S3	5
Figure S4	5
Figure S5	6
Figure S6	6
Figure S7	6
Table S3	7
Figure S8	7
Figure S9	8
Figure S10	8
Figure S11	8
Figure S12	9
Figure S13	9
Single Crystal X-Ray Diffraction (SCXRD)	
Table S4	10
Table S5	11
Table S6	12
Figure S14	13
Figure S15	13
X-ray Powder Diffraction (XRPD)	
Figure S16	14
Figure S17	15

Inductively Coupled Plasma-Optical Emission Spectroscopy (ICP-OES)

Instrumentation: ICP-OES analyses were performed with a ULTIMA 2 instrument HORIBA (Jobin Yvon, Longjumeau, France) in radial configuration, with a JY 2501 monochromator calibrated against carbon lines. Prior to the analysis each sample was dried under vacuum at room temperature. A certain amount of the obtained solid was therefore digested in 10 mL of HNO₃ 65% overnight. After digestion, the ligand was still insoluble, appearing as a white precipitate. The metal containing solution was therefore separated with a centrifuge, and then 0.77 mL of the solution were diluted with deionized water to obtain 25 mL of a 3 ppm metal solution in 2% HNO₃.

Table S1. Zn and Co concentration measured by ICP-OES analyses on sample of IRMOF-9 at different soaking time (Soaking conditions: 0.2 M CoCl₂ solution in N,N'-dimethylformamide at 305 K).

Soaking time (days)	Zn concentration (mg/L)	Co concentration (mg/L)
1	1.36 ± 0.03	0.91 ± 0.01
2	0.917 ± 0.002	1.318 ± 0.003
3	0.79 ± 0.02	1.48 ± 0.02
4	0.47 ± 0.01	1.77 ± 0.01
7	0.08 ± 0.03	2.03 ± 0.01
10	-	2.29 ± 0.02
15	-	2.54 ± 0.03



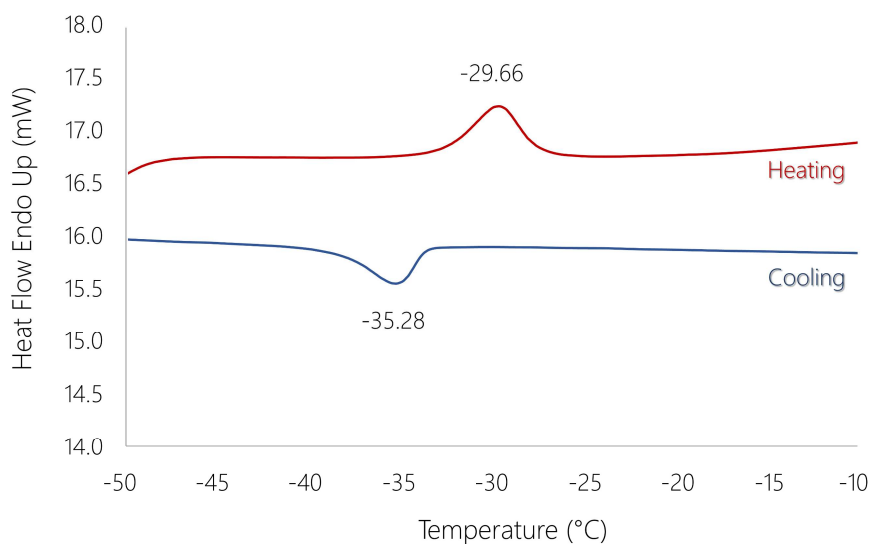
Graph S1. Plot of the molar fraction of Zn and Co as measured with ICP-OES analysis versus the soaking time of Zn-IRMOF-9 in a 0.2 M CoCl₂ solution at 305 K.

Table S2. Zn and Co concentration (mg/g) measured by ICP-MS analyses on sample of IRMOF-9(Co) after 30 days of soaking in a 0.2 M ZnCl₂ solution at 305K.

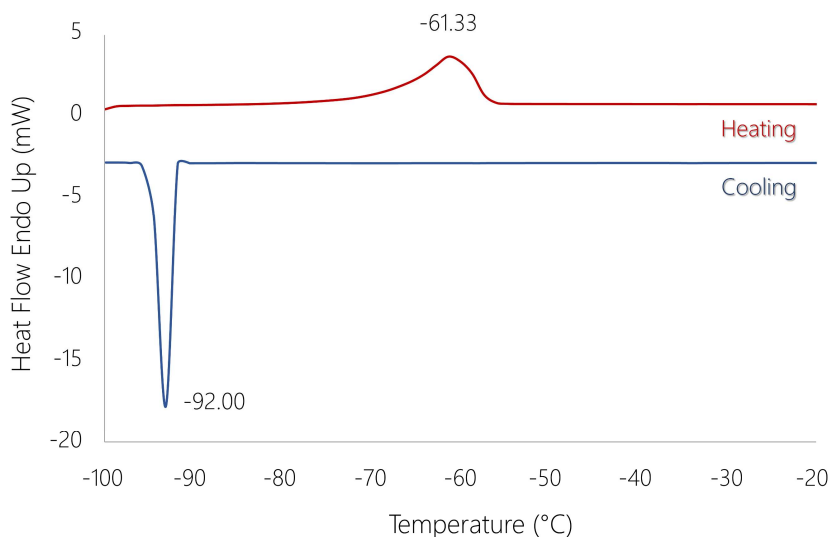
Sample	Co	Zn
IRMOF-9(Co) 30d	44,9 ± 0,5	260 ± 4

Differential Scanning Calorimetry (DSC)

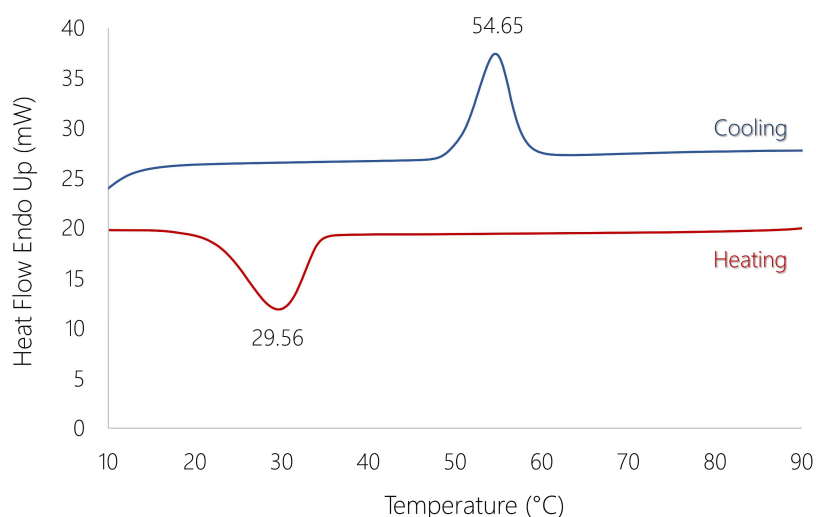
Instrumentation. DSC analyses on IRMOF-9(Co) and Co-1 were performed with a PerkinElmer DSC6000 equipped with Intracooler 6P cooling device and N₂ purging gas. Crystals were analysed in a dmf droplet to avoid their decomposition due to their instability to moisture. The samples were placed in a 50 μ L aluminium pan and a temperature ramp was applied from 303 K to 193 K, with a cooling rate of 5°C/min.



Graph S2. Thermal profile of IRMOF-9(Zn) in N,N'-dimethylformamide.



Graph S3. Thermal profile of IRMOF-9(Co) in N,N'-dimethylformamide.



Graph S4. Thermal profile of Co-1 and Co-2 in N,N'-dimethylformamide.

Optical Microscopy

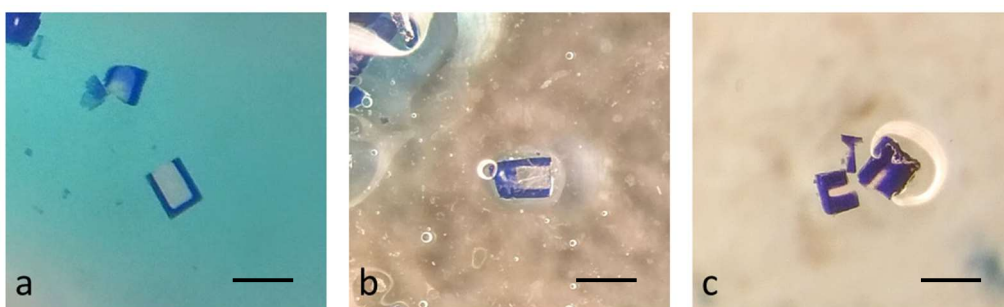


Figure S1. Optical microscope images of IRMOF-9(Zn) crystals after 7 (a), 14 (b) and 21 (c) days of soaking in a 0.2M CoCl_2 N,N'-dimethylformamide solution at 305 K. The specimens were cut to expose their section. The scale bar in every picture corresponds to 80 μm .

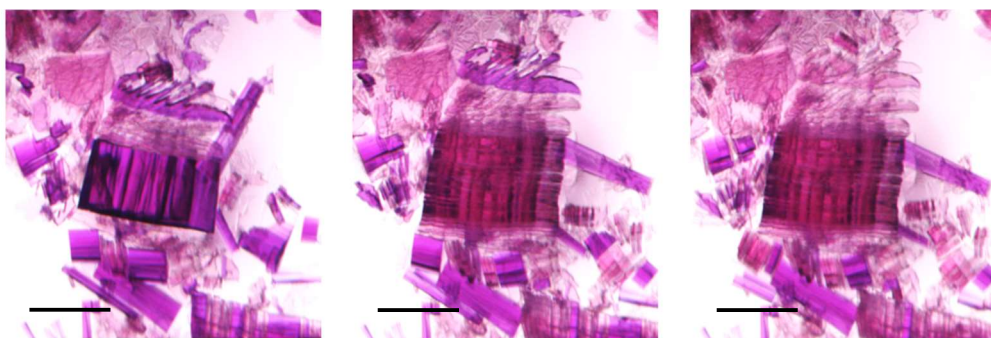


Figure S2. Crystals of Co-1 breaking in crystals of Co-2 in N,N'-dimethylformamide solution as the temperature cools down from 110°C to room conditions (from left to right). The scale bar in every picture corresponds to 50 μm .

Scanning Electron Microscopy (SEM)

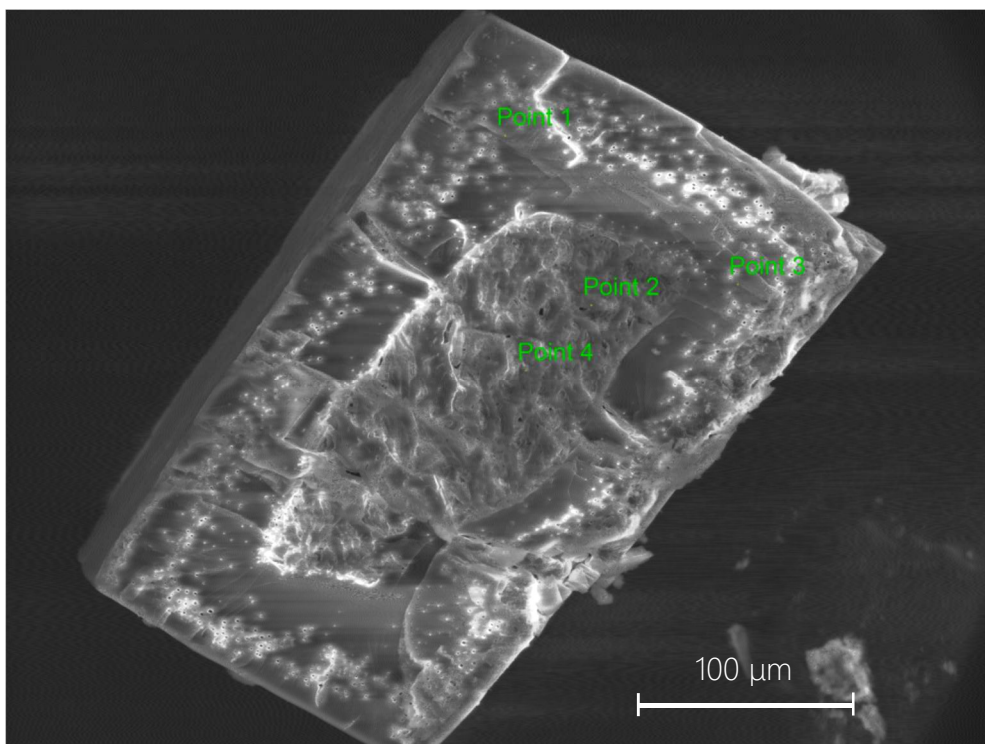


Figure S3. SEM image of the cut crystal used to perform elementary composition analyses (IRMOF-9 after 7 days of soaking in a 0.2M CoCl_2 N,N'-dimethylformamide solution at r.t.). In green: the points where the microanalyses were performed.

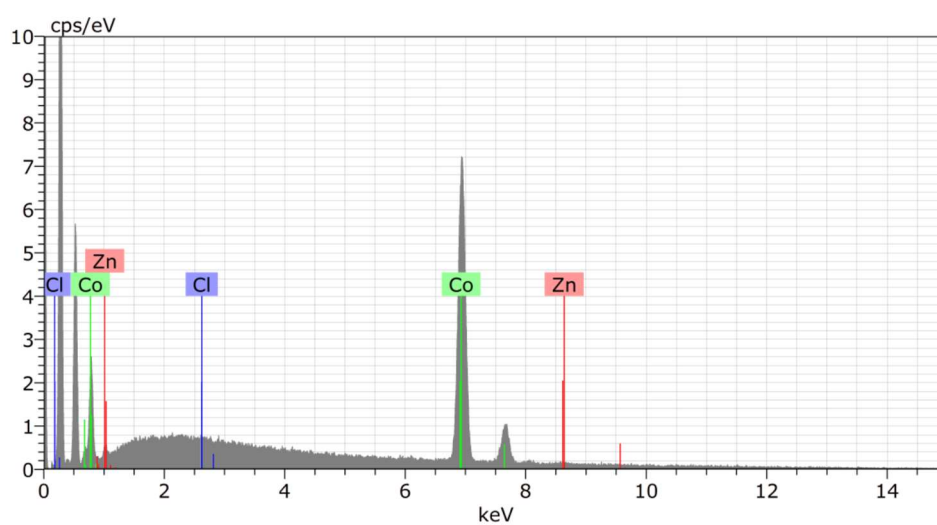


Figure S4. EDX spectrum for point 1 in figure 3.

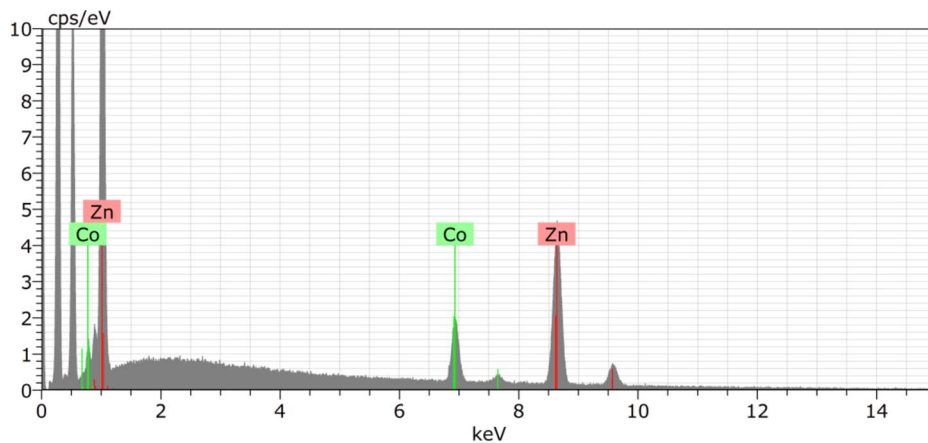


Figure S5. EDX spectrum for point 2 in figure 3.

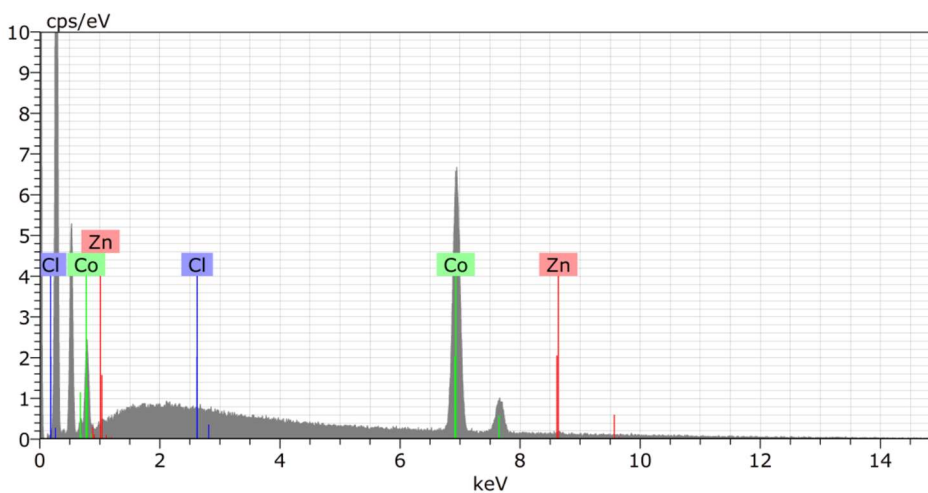


Figure S6. EDX spectrum for point 3 in figure 3.

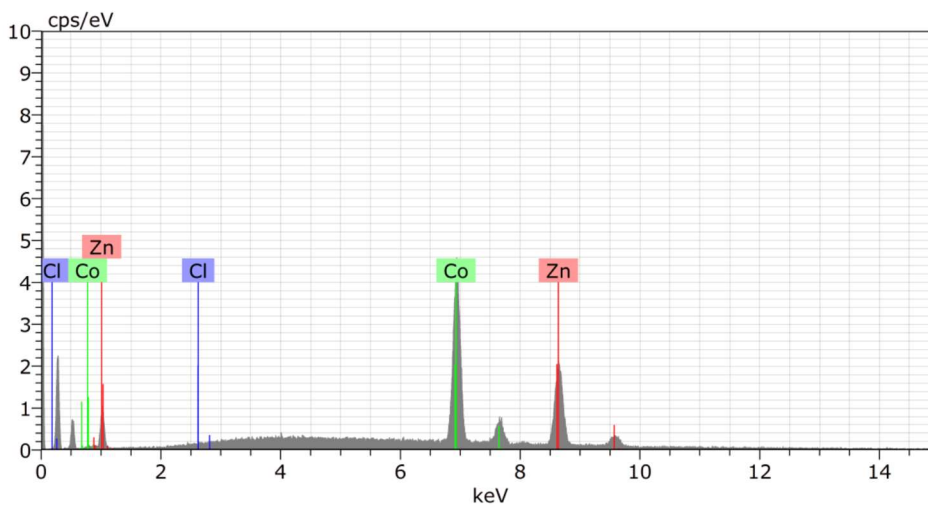


Figure S7. EDX spectrum for point 4 in figure 3.

Table S3. Summary of the normalized element abundance for points 1-4, relative to figure S4-7.

	point 1	point2	point 3	point 4
Zn at. %	12.61	87.58	47.11	93.03
Co at. %	86.43	12.42	52.63	6.76

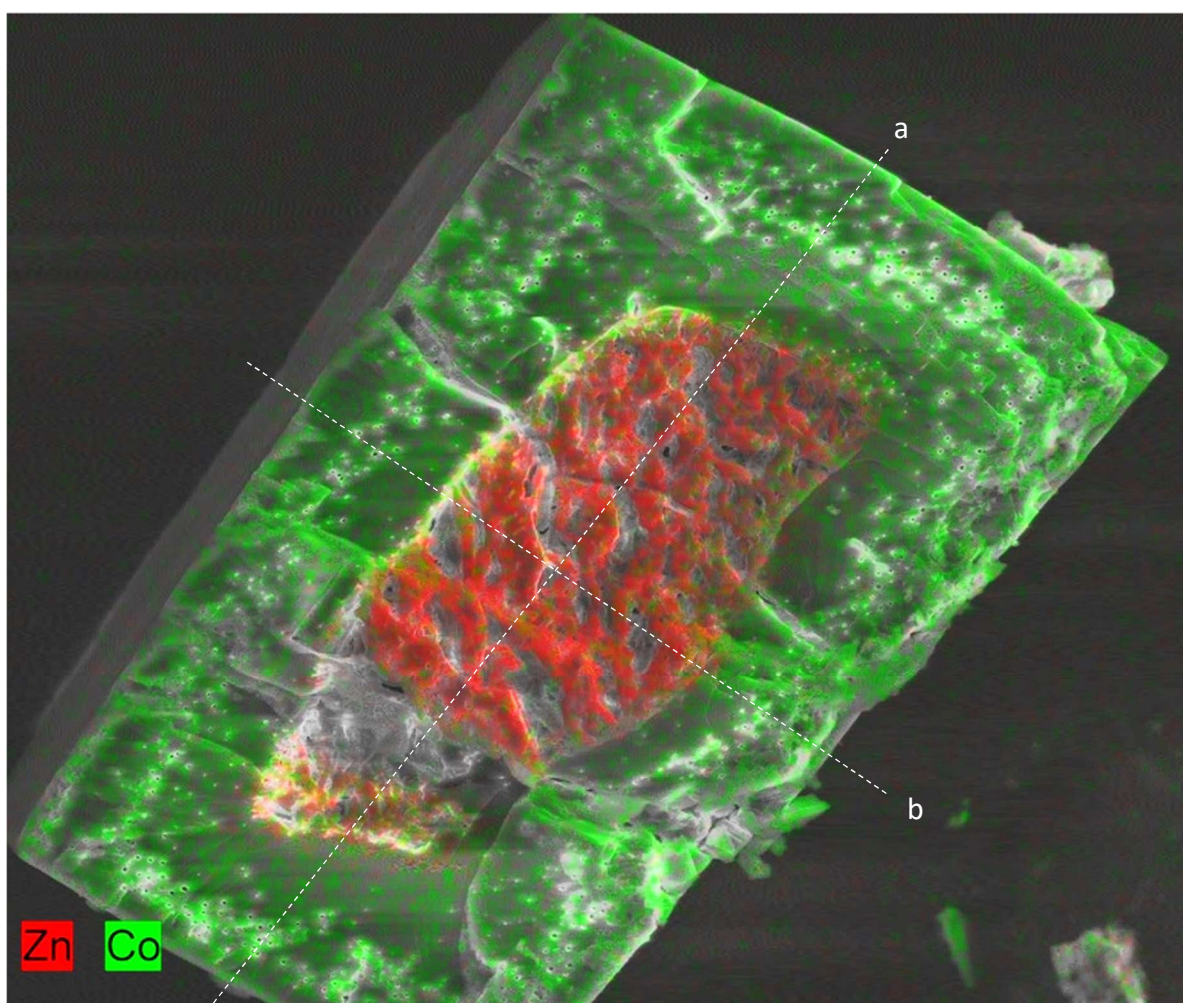


Figure S8. Colour map based on the EDX analyses of the Zn (red) and the Co (green) presence on the surface of the cut crystal shown in Figure S3. Part of this picture is shown in the main text of the paper in Figure 2. The two dashed lines are relative to the two elemental composition linear scans reported in Figures S9 and S10.

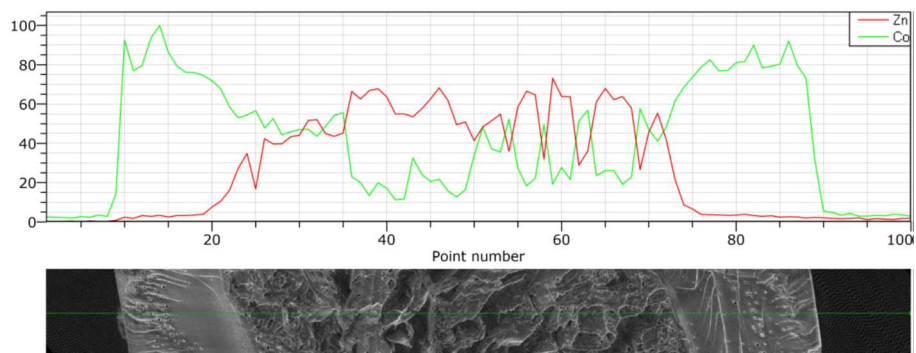


Figure S9. Line scan of Zn and Co abundance along the long section (dashed line a) of the cut crystal shown in Figure S8.

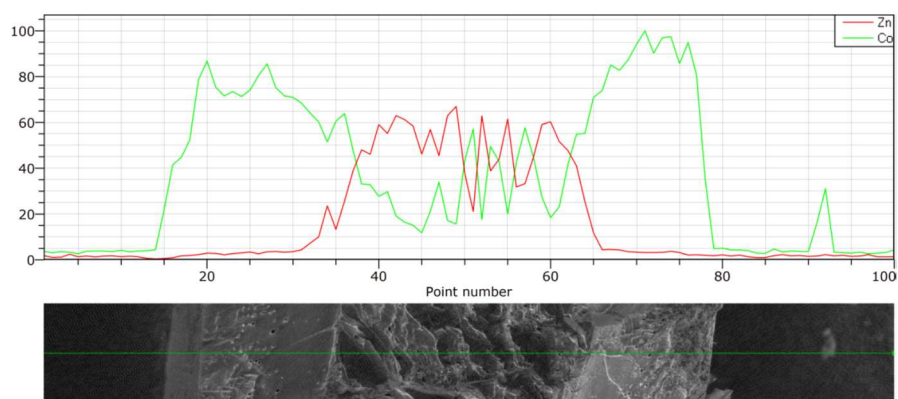


Figure S10. Line scan of Zn and Co abundance along the short section (dashed line b) of the cut crystal shown in Figure S8.

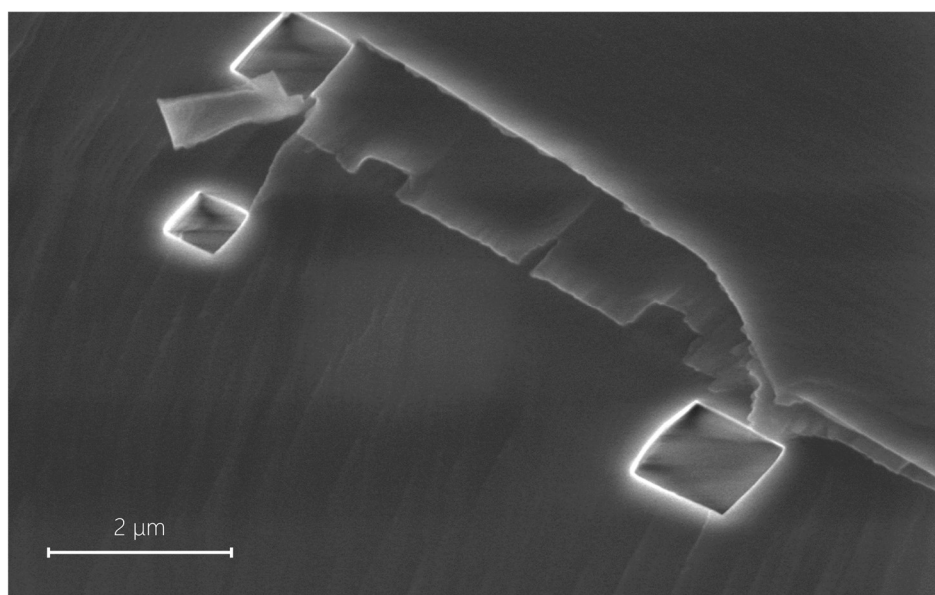


Figure S11. SEM micrograph of a selected region of the sample shown in Figure 2 in the main text, highlighting some μm -sized holes present in the inner section of the crystal.

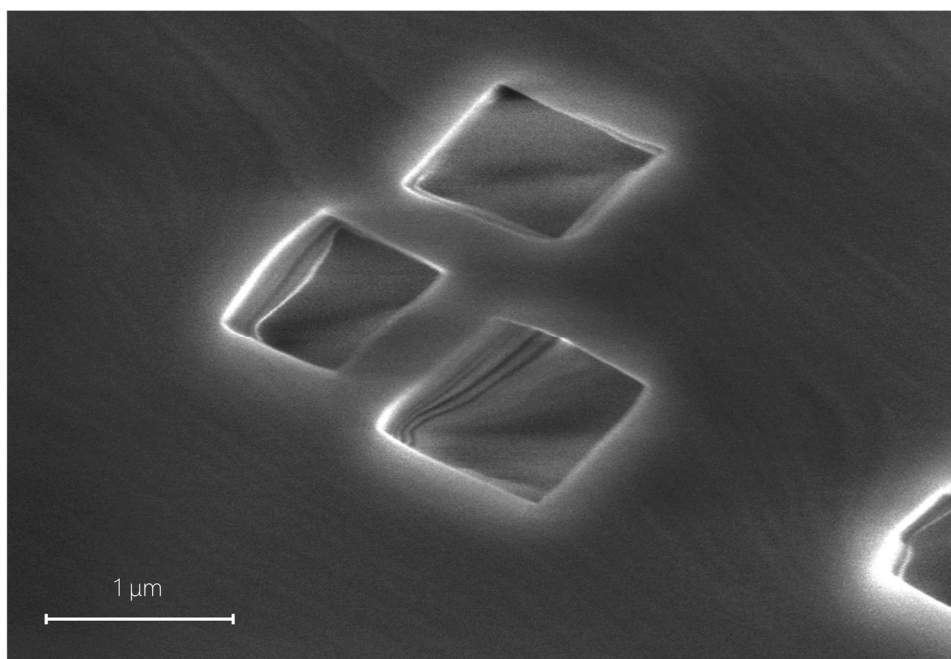


Figure S12. SEM micrograph of a selected region of the sample shown in Figure 2 in the main text, highlighting some μm-sized holes present in the inner section of the crystal.

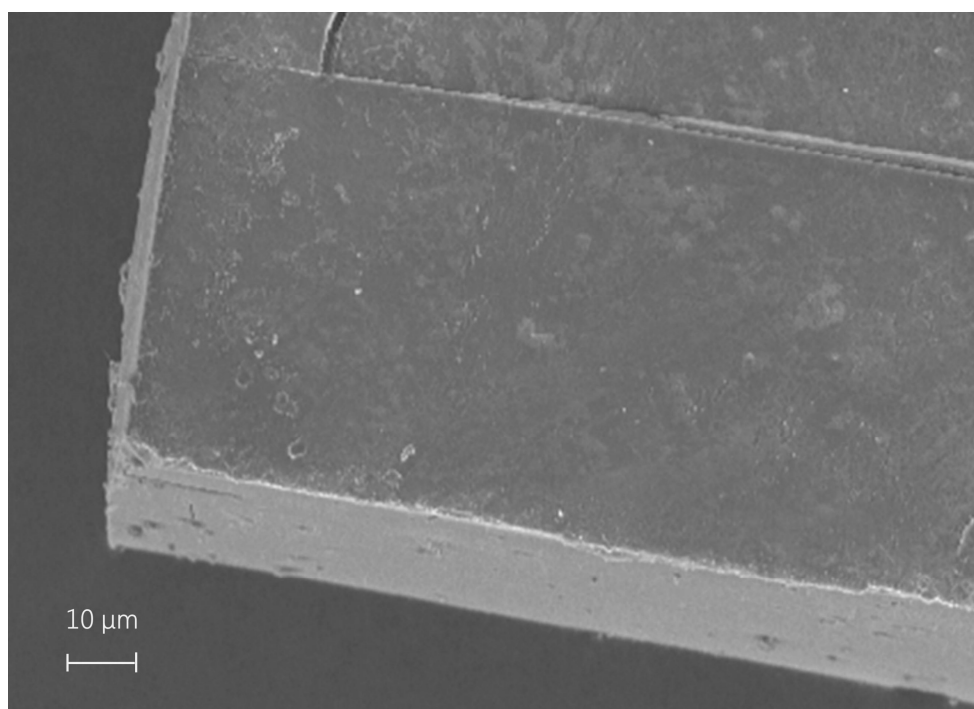


Figure S13. SEM image of the external surface of an IRMOF-9(Zn) crystal. The crystal was simply taken from the synthesis mother liquors, rinsed with fresh N,N'-dimethylformamide and deposited on the carbon tape for the SEM analysis.

Single Crystal X-Ray Diffraction (SCXRD)

Table S4. Crystal data and structure refinement for IRMOF-9(Co)

Identification code	IRMOF-9 (Co)
Empirical formula	C ₄₂ H ₂₄ Co ₄ O ₁₃
Formula weight	972.33
Temperature/K	258.0
Crystal system	orthorhombic
Space group	Pnmm
a/Å	17.1291(4)
b/Å	21.8862(5)
c/Å	26.2493(7)
α/°	90
β/°	90
γ/°	90
Volume/Å ³	9840.6(4)
Z	4
ρ _{calc} /cm ³	0.656
μ/mm ⁻¹	0.664
F(000)	1952.0
Crystal size/mm ³	0.3 × 0.2 × 0.2
Radiation	Synchrotron (λ = 0.700)
2θ range for data collection/°	2.974 to 45.766
Index ranges	-19 ≤ h ≤ 19, -24 ≤ k ≤ 24, -29 ≤ l ≤ 29
Reflections collected	86953
Independent reflections	7237 [R _{int} = 0.1167, R _{sigma} = 0.0526]
Data/restraints/parameters	7237/2513/705
Goodness-of-fit on F ²	1.142
Final R indexes [I ≥ 2σ (I)]	R ₁ = 0.1119, wR ₂ = 0.3473
Final R indexes [all data]	R ₁ = 0.1212, wR ₂ = 0.3705
Largest diff. peak/hole / e Å ⁻³	1.45/-1.00

The function “solvent mask” of the software Olex2 has been used to mask the residual electron density present in the channels, not possible to model due to the low data quality caused by the damages induced by the transmetalation. Solvent mask volume: 5729.9Å³. Electron count: 645.4.

Table S5. Crystal data and structure refinement for Co-1.

Identification code	Co-1
Empirical formula	C ₂₄ H ₁₉ Co _{1.5} NO ₇
Formula weight	521.80
Temperature/K	353.0
Crystal system	monoclinic
Space group	P2 ₁ /n
a/Å	11.0222(14)
b/Å	15.1754(19)
c/Å	19.331(3)
α/°	90
β/°	100.256(4)
γ/°	90
Volume/Å ³	3181.7(7)
Z	4
ρ _{calc} /cm ³	1.089
μ/mm ⁻¹	0.823
F(000)	1066.0
Crystal size/mm ³	0.65 × 0.4 × 0.4
Radiation	MoKα (λ = 0.71073)
2θ range for data collection/°	4.616 to 49.422
Index ranges	-12 ≤ h ≤ 12, -17 ≤ k ≤ 17, -22 ≤ l ≤ 22
Reflections collected	39837
Independent reflections	5397 [R _{int} = 0.0574, R _{sigma} = 0.0306]
Data/restraints/parameters	5397/0/302
Goodness-of-fit on F ²	1.033
Final R indexes [I ≥ 2σ (I)]	R ₁ = 0.0395, wR ₂ = 0.0892
Final R indexes [all data]	R ₁ = 0.0508, wR ₂ = 0.0937
Largest diff. peak/hole / e Å ⁻³	0.40/-0.34

The function “solvent mask” of the software Olex2 has been used to mask the residual electron density present in the channels, not possible to model due to the high disorder caused by the relatively high temperature conditions maintained during the data collection. Solvent mask volume: 1234.8Å³. Electron count: 211.3.

Table S6. Crystal data and structure refinement for Co-2.

Identification code	Co-2
Empirical formula	C ₆₃ H ₇₃ CO ₃ N ₇ O ₁₉
Formula weight	1409.07
Temperature/K	100.0
Crystal system	monoclinic
Space group	Pn
a/Å	13.1391(7)
b/Å	13.3582(6)
c/Å	19.7524(10)
α/°	90
β/°	106.272(2)
γ/°	90
Volume/Å ³	3328.0(3)
Z	2
ρ _{calc} /g/cm ³	1.406
μ/mm ⁻¹	0.815
F(000)	1466.0
Crystal size/mm ³	0.2 × 0.2 × 0.1
Radiation	MoKα (λ = 0.71073)
2θ range for data collection/°	4.296 to 52.74
Index ranges	-16 ≤ h ≤ 16, -16 ≤ k ≤ 16, -24 ≤ l ≤ 24
Reflections collected	135826
Independent reflections	13622 [R _{int} = 0.0585, R _{sigma} = 0.0283]
Data/restraints/parameters	13622/2/844
Goodness-of-fit on F ²	1.025
Final R indexes [I >= 2σ (I)]	R ₁ = 0.0268, wR ₂ = 0.0601
Final R indexes [all data]	R ₁ = 0.0342, wR ₂ = 0.0635
Largest diff. peak/hole / e Å ⁻³	0.34/-0.37
Flack parameter	0.007(3)

The phase is found affected by merohedral twinning, likely caused by the symmetry break due to the Co-1 → Co-2 phase transition. Twinning law: (-1.0, 0.0, 0.0, 0.0, -1.0, 0.0, 0.0, 0.0, -1.0); BASF: 0.344(11).

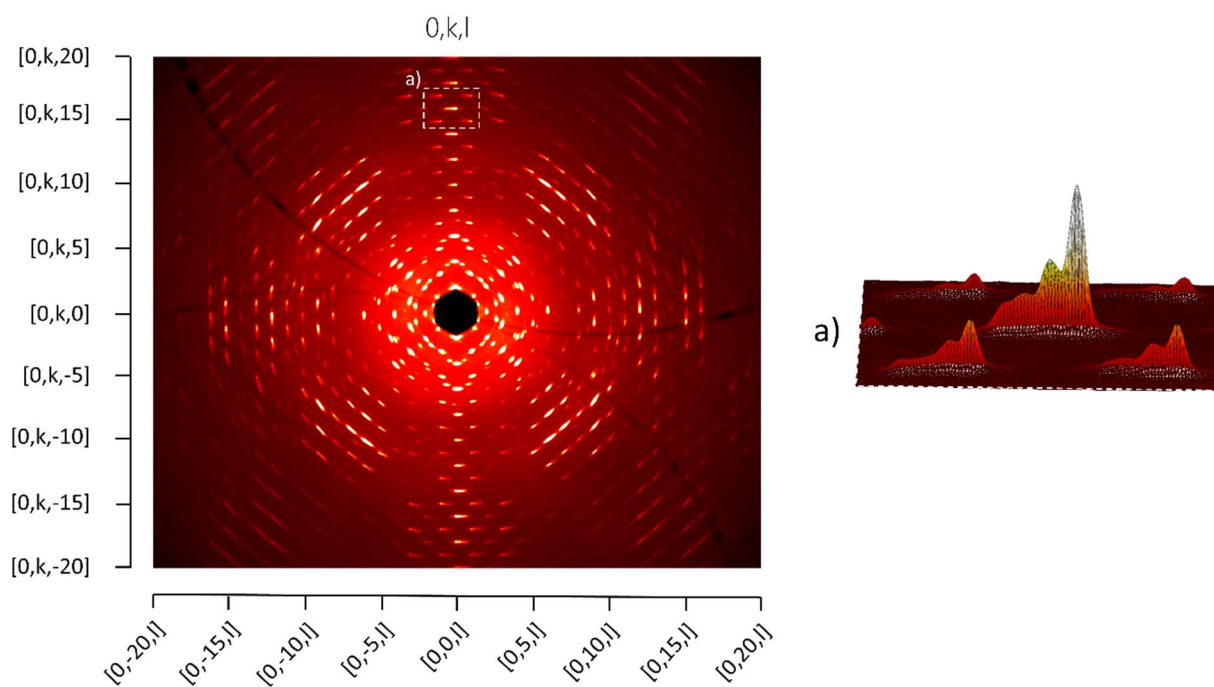


Figure S14. Reconstruction of the (0 k l) plane of IRMOF-9(Co) reciprocal space from Single Crystal XRD data. The damaged crystallinity is evident from the shape of the Bragg reflections, elongated concentrically with respect to the origin of the reciprocal lattice. In the 3D visualisation of the intensities relative to the box marked in dashed line (a) it is possible to notice that the specimen consists of mainly 4 domains slightly displaced with each other. At low $q(r^*)$ additional reflections are likely due to a small fragment detached from the main crystal body.

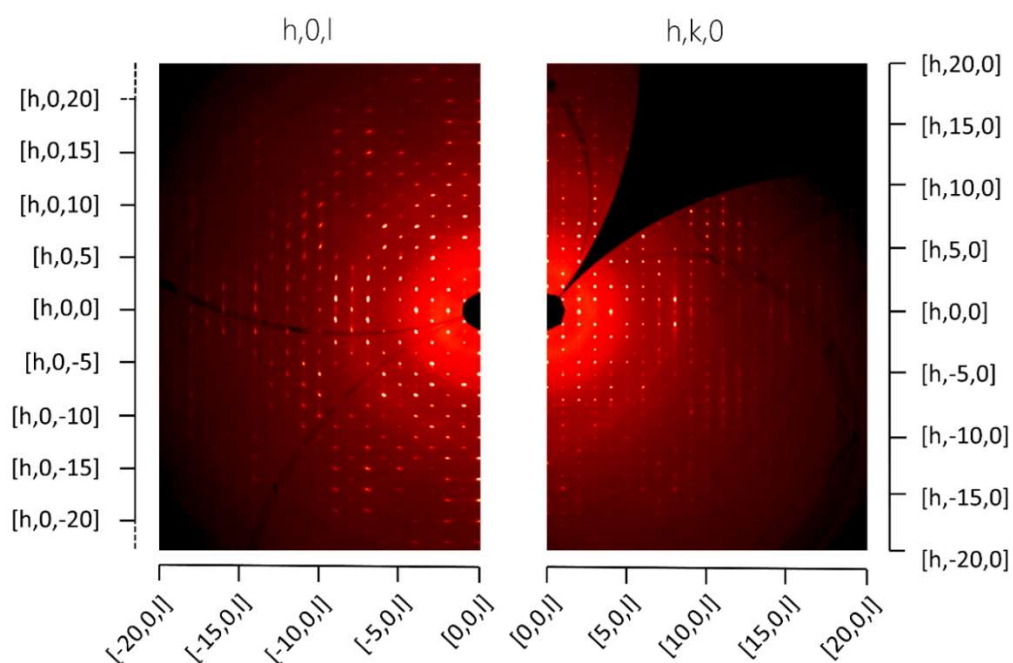


Figure S15. Reconstruction of part of the (h, 0, l) and (h, k, 0) planes of IRMOF-9(Co) reciprocal space. Weak but recognisable diffuse scattering lines lie along the b^* and c^* directions, corresponding to a decrease in the translational symmetry along the b and c crystallographic axes. As explained in the main text, these axes are those orthogonal to the channel axis, which runs along the a crystallographic direction.

X-Ray Powder Diffraction (XRPD)

X-ray powder diffraction patterns of IRMOF-9(Zn) and completely transmetalated IRMOF-9(Co) were acquired at the XRD1 beamline of the Elettra Synchrotron (CNR Trieste). The completeness of the transmetalation has been confirmed by ICP-OES analyses.

The data were collected at 250K in transmission using a 0.7Å radiation. In each sample preparation, a 0.7mm glass capillary was filled with pure N,N'-dimethylformamide and only then crystals of the sample were inserted and packed in the capillary. This procedure was adopted to avoid the contact of the two phases with air in order to avoid their decomposition due to reaction with moisture.

The diffracted intensities were detected by a Pilatus 2M detector. The resulting 2D diffraction images were converted in the XRD profile by using the "Powder power tool" of the CrysAlisPro Software package. XRD profiles have been generated by using the OriginPro software (v. 8.0724).

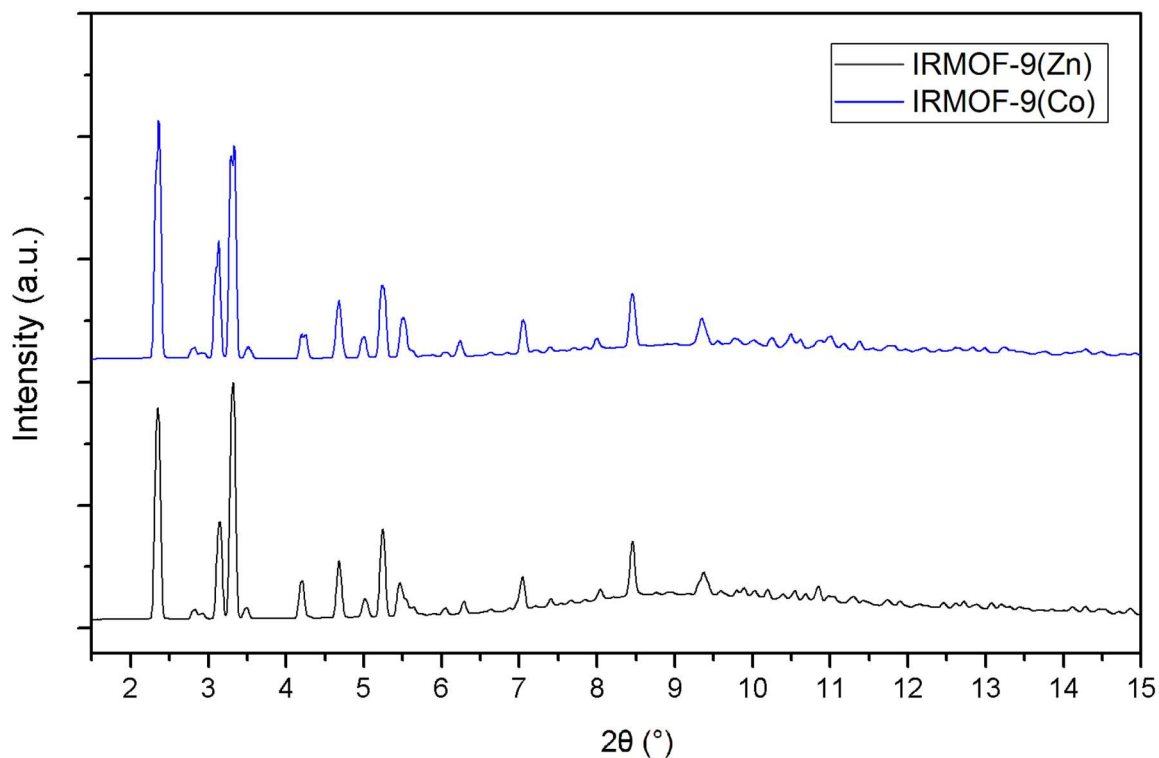


Figure S16. Stacked XRPD patterns of IRMOF-9(Zn) and IRMOF-9(Co).

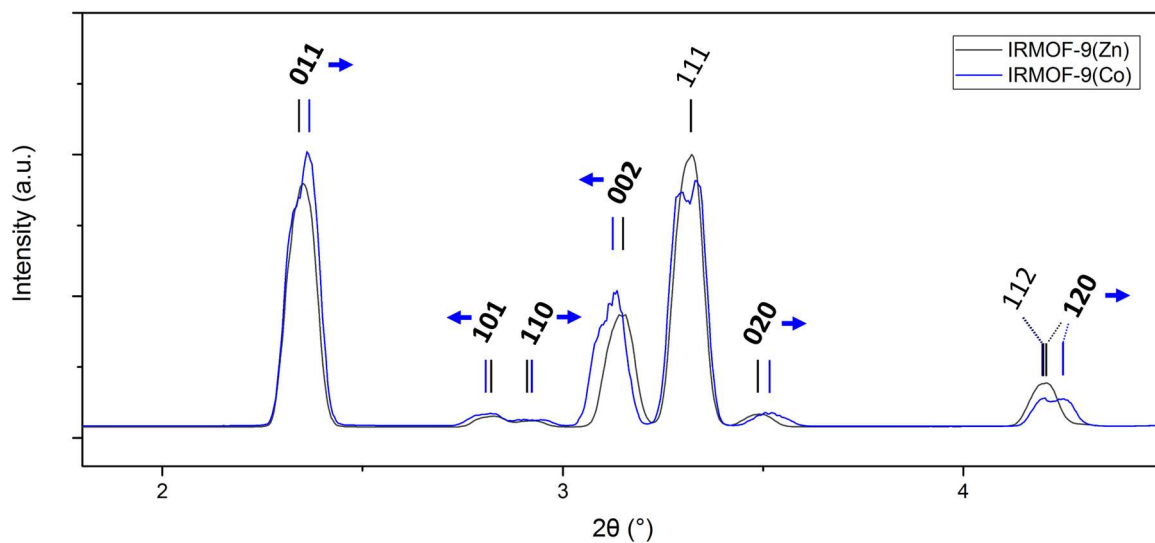


Figure S17. Superimposed XRPD patterns of IRMOF-9(Zn) and IRMOF-9(Co). The highlighted reflections are the ones that are more affected by the lattice deformation induced by the transmetalation. In detail, the reflections containing an important contribution of the k or l Miller indices are shifted to the right or to the left respectively, consistently with the decrease of the b axis length and increase of the c axis length after the Zn-to-Co exchange. Overall, the peak shape in the IRMOF-9(Co) pattern is more irregular and asymmetrical. This effect is likely due to the observed lattice disorder, which reasonably causes deviations of the lattice parameters from the average ones in different zones of the single crystals, and in different crystals.